

The Extinction-to-Backscatter Ratio of Tropospheric Aerosol: A Numerical Study

JÖRG ACKERMANN

Meteorologisches Institut, Universität München, Munich, Germany

12 May 1997 and 7 October 1997

ABSTRACT

An adequate estimation of the aerosol extinction-to-backscatter ratio S is important for solving the underdetermined single scattering lidar equation and for investigating the climate impact of aerosols. In this study, the extinction-to-backscatter ratios for the Nd:YAG wavelengths are calculated for continental, maritime, and desert aerosols; the corresponding aerosol components are varied within the expected natural variabilities of the particle number mixing ratios.

For continental aerosol, S increases with the relative humidity f from 40 to 80 sr. For maritime aerosol, the extinction-to-backscatter ratios lie between 15 and 30 sr for 355 and 532 nm and between 25 and 50 sr for 1064 nm. The desert aerosol exhibits a weak dependence of S on f and ranges between 42 and 48 sr for 355 nm and between 17 and 25 sr for 532 and 1064 nm. For practical applications, the calculated values of S are fitted by a power series expansion with respect to their dependence on f .

1. Introduction

Backscatter lidar measurements are considered useful for the derivation of atmospheric extinction profiles. However, the backscatter lidar equation is underdetermined due to its dependence on the two unknowns, backscatter coefficient and extinction coefficient (e.g., Klett 1981, 1985; Hughes et al. 1985; Sasano et al. 1985; Bissonnette 1986; Kovalev 1993). This dependence necessitates the prescription of the ratio between the aerosol extinction coefficient and the aerosol backscatter coefficient, that is, the lidar ratio.

Since the lidar ratio connects two optical quantities that both depend on the wavelength of the incident light, the refractive index, and the aerosol size distribution, its behavior is not obvious: in real atmospheres, aerosol is a mixture of different components and hence different refractive indices. Each of these components has a distinct size distribution, which, assuming it is lognormally distributed, is defined by its median radius and the width of the distribution. Therefore, the combination of different aerosol components with different chemical properties and size distributions is manifold.

In addition, some aerosol components change their size distributions and refractive indices due to variations of the relative humidity. Since the relative humidity increases often with altitude within the planetary boundary layer (PBL), the physical-chemical properties of the

particles are height dependent. Thus, for the measurements with an upward-looking monostatic lidar system, due to the change of the relative humidity along the measurement path, the lidar ratio may differ considerably from an assumed constant range-independent value. It is one of the objectives of this study to quantify this variability for different aerosol types by numerical simulations.

Since the extinction-to-backscatter ratio is also important in estimating the climate impact of aerosols, there are several studies of an experimental determination of the lidar ratio. The results are manifold: using the slope method, Saleminck et al. (1984) found a linear increase of the lidar ratio from about 25 to 70 sr between 40% and 80% relative humidity near the surface. They reported no significant difference between 532 and 1064 nm. Combining lidar, sun photometer, and optical particle counter measurements, Takamura et al. (1994) derived values between 20 and 70 sr for 532 nm. Waggoner et al. (1972) retrieved an aerosol scatter-to-backscatter ratio of about 84 sr for relative humidities less than 75% using nephelometer data at 680 nm and ruby lidar data at 694 nm. From ruby lidar slant path measurements, Spinhirne et al. (1980) deduced an average extinction-to-backscatter ratio of 19.5 sr for the PBL near Tucson, Arizona. The most actual data are published by Rosen et al. (1997): from a combination of nephelometer and backscatter sonde measurements a mean extinction-to-backscatter ratio of 41.6 sr at 490 nm and 32.2 sr at 700 nm is calculated for near-surface aerosols over the southwestern United States.

In case of elastic backscattering, range-dependent values of the lidar ratio are known only theoretically, when

Corresponding author address: Dr. Jörg Ackermann, MIM - Meteorologisches Inst., Universität München, Theresienstr. 37, 80333 München, Germany.
E-mail: uh234aj@mail.lrz-muenchen.de

the physical–chemical properties and the size distribution of the aerosol particles along the lidar line are known. However, the fulfillment of these requirements would make the lidar measurements unnecessary. Thus, the lidar ratio must be estimated with respect to the measurement site and to any available a priori information about the actual state of the atmosphere.

The a priori information about the actual temperature–pressure relationship, and hence the Rayleigh backscattering and extinction properties of the atmosphere, is often determined from nearby routine measurements (e.g., radiosonde ascents). In these cases one also has information about the vertical humidity profile, which for the majority of atmospheric conditions is one of the most important prerequisites for the lidar ratio estimation.

From the geographical location of the measurement site, it is possible to perform a crude preselection of the aerosol type: over continents, mainly three components occur (water soluble, insoluble, and soot particles); over oceans, the aerosol consists of sea salt, water soluble; in coastal regions there are additional soot particles; and over deserts, minerals in combination with water soluble particles are present. Hence, the variability of aerosols results mainly from the fact that for one aerosol type, the mixing ratios of the distinct components are unknown. On the basis of this assumption, this study is a systematic and extensive numerical investigation about the lidar ratio of tropospheric aerosols. The physical basis and the input data are presented in sections 2 and 3, respectively. The results for the different aerosol types are discussed separately in sections 4 to 6, whereby the main emphasis is put on the calculation of the lidar ratio for varying aerosol components and different relative humidities.

2. Physical basis

In the following considerations, it is assumed that the aerosol is an external mixture of internally mixed components. Each aerosol component (index i) is lognormally distributed with respect to the particle radius r :

$$n_i(r) = \frac{N_i}{(2\pi)^{1/2} \ln \sigma_i r} \exp \left[-\frac{\ln^2(r/r_{m,i})}{2 \ln^2 \sigma_i} \right] \quad (1)$$

where N_i is the number density of the component, and $r_{m,i}$ and σ_i denote the median radius and the standard deviation of $n_i(r)$, respectively.

The number mixing ratio μ_i (i.e., the normalized number particle concentration) is defined as

$$\mu_i = \frac{N_i}{\sum_{i=1}^M N_i} = \frac{N_i}{N_{\text{tot}}} \quad (2)$$

Here, M is the number of aerosol components and N_{tot} is the total number of particles per unit volume. Com-

binning Eqs. (1) and (2), the lognormal distribution can be expressed by

$$n_i(r) = \frac{N_{\text{tot}} \mu_i}{(2\pi)^{1/2} \ln \sigma_i r} \exp \left[\frac{-\ln^2(r/r_{m,i})}{2 \ln^2 \sigma_i} \right]. \quad (3)$$

The following considerations refer to $N_{\text{tot}} = 1 \text{ cm}^{-3}$.

For a given wavelength λ the optical quantities of each component depend on the radius r and the refractive index m_i . Due to the influence of relative humidity, the hygroscopic aerosol components change their refractive index (Hänel 1976):

$$m_i = m_w + (m_{0,i} - m_w) \left(\frac{r_{0,i}}{r_{m,i}} \right)^3. \quad (4)$$

In Eq. (4), m_w denotes the refractive index of water, and $m_{0,i}$ is the refractive index of the dry particle of component i with the median radius $r_{0,i}$. The exponent indicates that Eq. (4) describes a volume-weighted average of refractive indices of water and the considered component.

By means of Mie theory, the extinction efficiency $Q_{\text{Ext},i}(r, m_i, \lambda)$ and the backscatter efficiency $Q_{\text{Back},i}(r, m_i, \lambda)$ can be calculated. This procedure is repeated for each aerosol component. Accordingly, the resulting lidar ratio S is given by

$$S = \frac{\sum_{i=1}^M \int_0^\infty Q_{\text{Ext},i}(r, m_i, \lambda) \pi r^2 n_i(r) dr}{\sum_{i=1}^M \int_0^\infty Q_{\text{Back},i}(r, m_i, \lambda) \pi r^2 n_i(r) dr}, \quad (5)$$

where the numerator expresses the extinction contribution α_i and the denominator the backscatter contribution β_i , that is,

$$S = \frac{\int_0^\infty \sum_{i=1}^M \alpha_i dr}{\int_0^\infty \sum_{i=1}^M \beta_i dr}. \quad (6)$$

Figure 1 illustrates an example for the calculation of the lidar ratio. A continental aerosol, which consists of the three components water soluble, soot, and insoluble, is chosen (Fig. 1a). The relative humidity, which influences the microphysical properties of the water soluble component, is assumed to be 90%, and the wavelength of the incident light is 532 nm.

With knowledge of the refractive indices, the extinction efficiencies and backscatter efficiencies are calculated. These quantities are weighted with the size distribution of the corresponding aerosol component. To obtain the extinction and backscattering for a distinct particle radius, the contributions of the three aerosol components are summed. The resulting curves are plotted in Fig. 1b. From the maxima of the curves note that,

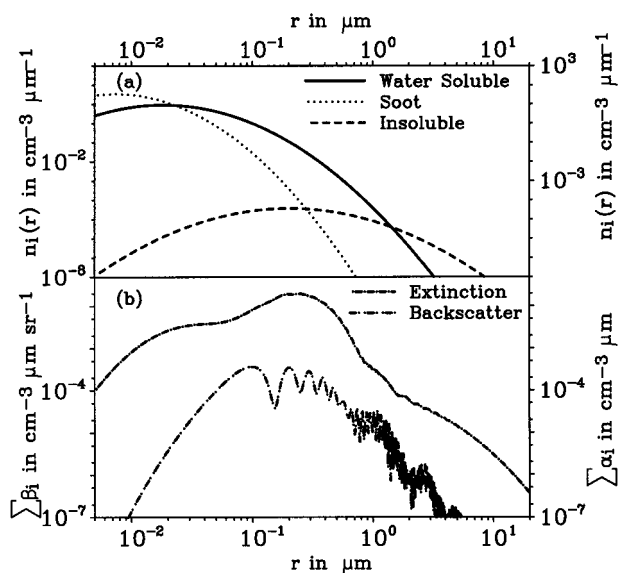


FIG. 1. Determination of the lidar ratio for a three-component aerosol. (a) The size distributions. (b) Backscatter and extinction are summed for the distinct components.

the main contribution to both backscattering and extinction at 532 nm comes from particles with radii between 0.1 and 0.6 μm . The resulting lidar ratio is the ratio of the integrals of the extinction curve and the backscatter curve shown in Fig 1b.

The procedure described above is repeated for each combination of aerosol components discussed in the following sections.

3. Input data

As input for the Mie calculations, aerosol climatology data from Hess et al. (1998), based on prior climatologies of d'Almeida et al. (1991) and Shettle and Fenn (1979), are used. These climatologies include for each aerosol component the refractive index m ($m = \eta - i\kappa$), the median radii r_m for different relative humidities f , and the standard deviation σ of the corresponding lognormal distribution. The wavelengths considered in this study are 1064 nm (near infrared), 532 nm (visible), and 355 nm (near UV), which are the fundamental, doubled, and tripled wavelengths of an Nd:YAG laser.

For the aerosol components used in this study the

input parameters are summarized in Tables 1 and 2. Briefly, the chemical compositions of the components are as follows: the water soluble particles consist mainly of nitrate and sulfate and have no distinct sources (Hess et al. 1998). The chemical composition of insoluble particles is manifold since they originate from different soils or plants or man-made activities. Soot is generated in all kinds of combustion and is supposed to be graphitic carbon. Sea salt consists mainly of sodium chloride, but also of other kinds of salt, that occur in seawater. The mineral component is a mixture of quartz and clay. The chainlike character of soot particles is not accounted for. Instead, one soot particle is considered as one primary particle of such a chain. Compared to the representation of a soot particle as a cluster, the number concentration of the particles is enlarged, and the mode radius of the corresponding size distribution is very small.

The internal variabilities of the distinct components make clear that the refractive indices given in Table 1 do not refer to one distinct chemical composition but rather to a mixture of different substances. Consequently, external mixing of the components must be seen as external mixing of internally mixed components.

The Mie code of Bohren and Huffman (1983) is applied to the aerosol data. The possible nonsphericity of the particles is not respected. This simplification can cause serious errors for all nonhygroscopic components, especially when the particles are large compared to the wavelength of the incident light.

It is expected that the measurements of continental aerosols are most common. Thus, the calculated lidar ratios for the continental aerosol will be discussed in more detail than the results for the maritime aerosol and the desert aerosol.

4. Continental aerosol

The continental aerosol type consists of the three components: insoluble, soot, and water soluble. The median radius of the latter component grows with increasing relative humidity (see Table 2).

For given optical properties and a distinct relative humidity, the variability of the lidar ratio is caused by different number mixing ratios. Consequently, it is necessary to consider a wide range of possible combinations of number mixing ratios with the boundary condition

TABLE 1. The real parts (η) and imaginary parts (κ) of the refractive indices for the aerosol components used in this study. The subscripts denote the three considered wavelengths in nanometers.

Component	η_{355}	κ_{355}	η_{532}	κ_{532}	η_{1064}	κ_{1064}
Water soluble	1.530	5.00×10^{-3}	1.530	5.64×10^{-3}	1.520	1.64×10^{-2}
Insoluble	1.530	8.00×10^{-3}	1.530	8.00×10^{-3}	1.510	8.00×10^{-3}
Soot	1.750	4.64×10^{-1}	1.750	4.46×10^{-1}	1.760	4.43×10^{-1}
Mineral	1.530	1.66×10^{-2}	1.530	6.33×10^{-3}	1.530	4.30×10^{-3}
Sea salt	1.510	3.22×10^{-8}	1.500	1.12×10^{-8}	1.470	1.95×10^{-4}
Water	1.343	6.00×10^{-9}	1.333	1.61×10^{-9}	1.326	1.39×10^{-5}

TABLE 2. The parameters of the lognormal distributions for different relative humidities of the aerosol components used in this study. The unity of r_m is in micrometers (Hess et al. 1998).

Component	r_m (0%)	r_m (50%)	r_m (70%)	r_m (80%)	r_m (90%)	r_m (95%)	r_m (98%)	r_m (99%)	σ
Water soluble	0.0212	0.0262	0.0285	0.0306	0.0348	0.0399	0.0476	0.0534	2.239
Insoluble	0.4710	0.4710	0.4710	0.4710	0.4710	0.4710	0.4710	0.4710	2.512
Soot	0.0118	0.0118	0.0118	0.0118	0.0118	0.0118	0.0118	0.0118	2.000
Mineral (nuc.)	0.0700	0.0700	0.0700	0.0700	0.0700	0.0700	0.0700	0.0700	1.950
Mineral (acc.)	0.3900	0.3900	0.3900	0.3900	0.3900	0.3900	0.3900	0.3900	2.000
Mineral (coa.)	1.9000	1.9000	1.9000	1.9000	1.9000	1.9000	1.9000	1.9000	2.150
Sea salt (acc.)	0.2090	0.3360	0.3780	0.4160	0.4970	0.6050	0.8010	0.9950	2.030
Sea salt (coa.)	1.7500	2.8200	3.1700	3.4900	4.1800	5.1100	6.8400	8.5900	2.030

that the sum of these mixing ratios equals 1. In the following, the mixing ratios for water soluble, insoluble, and soot particles are denoted μ_1 , μ_2 , and μ_3 , respectively.

The mixing ratio μ_1 is varied between 0.1 and 1 in steps of 0.1. Accordingly, since μ_2 is about four orders less, μ_3 has values between 0.9 and 0. To account for the influence of the insoluble component, μ_2 is varied between 6×10^{-6} and 6×10^{-5} in steps of 6×10^{-6} . Compared to the composition of the standard aerosol types proposed by Hess et al. (1998), it is expected that the choice of these 100 different combinations covers the high variability of the aerosol that can occur over

continental areas. The high soot content of 0.9 is of the same order of magnitude as the value of 0.823 proposed by Hess et al. (1998) for the aerosol type “urban.”

To respect the influence of the relative humidity f on the water soluble component and hence on the lidar ratio, the calculations are performed for relative humidities of 0%, 50%, 70%, 80%, 90%, 95%, 98%, and 99%, respectively.

Figure 2 shows the calculated mean lidar ratios \hat{S} and the deviations from \hat{S} for relative humidities of 0%, 50%, 90%, and 99%, and for the wavelengths 355, 532, and 1064 nm, respectively. These nine contour plots enable us to investigate in detail the influence of the three aerosol components on the values of S .

For all three wavelengths, the variabilities of S have their maxima at $f = 0\%$. In particular, a high soot content can cause large positive deviations of the lidar ratio from its mean value. This result is due to the large imaginary part of the refractive index and hence the extinction of these particles. For 1064 nm, this effect can be compensated or even exceeded by a high amount of insoluble particles (see Fig. 2 at the lower left).

The contributions of the three different components to the lidar ratio can be estimated from the slopes of the isolines in Fig. 2. When the absolute of the slopes is near zero, the influence of the mixing ratios of soot and water soluble particles is small, whereas when the absolute of the slopes grows to infinity, the insoluble component has hardly any influence on S . Thus, the mixing ratio of the insoluble particles has for all relative humidities a small influence on the lidar ratio for 355 nm. In contrast, the change of the insoluble component plays the dominant role for the variability of the lidar ratio at 1064 nm.

The standard deviation s of the lidar ratio is calculated for each wavelength and relative humidity. The result is shown in Fig. 3. The error bars of length $2s$ at a definite relative humidity must be regarded as the variability of the lidar ratio driven by the assumption made on the variability of the distinct values of μ_1 , μ_2 , and μ_3 .

Since the water soluble component is the only component whose properties are affected by the relative humidity, all variations of \hat{S} and s with respect to their values for $f = 0\%$ are considered as variations of the

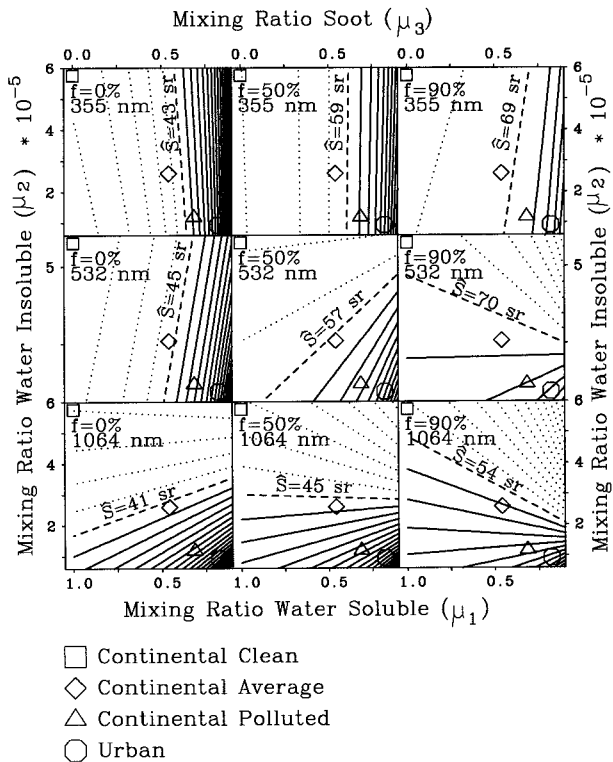


FIG. 2. Deviations of the calculated lidar ratios from the mean values of \hat{S} for 355, 532, and 1064 nm and relative humidities of 0%, 50%, and 90%. The dotted, dashed, and full lines indicate negative, zero, and positive deviations from \hat{S} , respectively, and the contour interval is 1 sr. The mixing ratios of the four standard aerosol types proposed by Hess et al. (1998) are shown by open symbols.

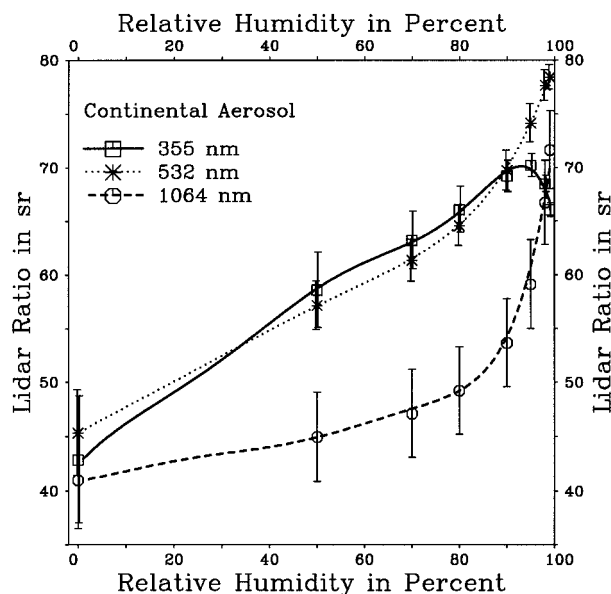


FIG. 3. Dependence of the lidar ratios on the relative humidity for different wavelengths for continental aerosol. The curves are the results of power series expansions, the symbols indicate the calculated values of \hat{S} , and the error bars are calculated on the assumptions made about the variabilities of the distinct components.

water soluble component. The change of \hat{S} and s due to increasing f has two causes: first, a decrease of the real and the imaginary part of the refractive index and second, a shift of the lognormal distribution to larger radii due to the growth of the particles (Fitzgerald 1984). Since in most cases the extinction increases, in general the latter effect is dominant.

For relative humidities up to 95%, there are only small differences between \hat{S} for 355 nm and \hat{S} for 532 nm. For larger relative humidities, the lidar ratio increases at 532 nm and decreases at 355 nm. This decrease is caused by the strong increase of the backscatter coefficient at 355 nm due to the growth of the water soluble particles. For $f < 95\%$, the decrease of extinction with increasing wavelength is the governing effect that causes the lidar ratio for 1064 nm to be smaller than for 355 nm and for 532 nm. The high variability of \hat{S} with f suggests that the physical-chemical properties of the water soluble particles dominate over the influence of soot and insoluble particles.

The calculated uncertainties for the different wavelengths decrease with increasing relative humidity: for 355 nm, the uncertainties range from $\pm 1\%$ to $\pm 14\%$, for 532 nm from $\pm 1\%$ to $\pm 9\%$, and for 1064 nm from $\pm 5\%$ to $\pm 11\%$.

5. Maritime aerosol

The maritime aerosol occurs in the PBL over oceans and over nearby coastal regions. It is composed of four components: water soluble, soot, and the accumulation and the coarse mode of sea salt. The particles of the

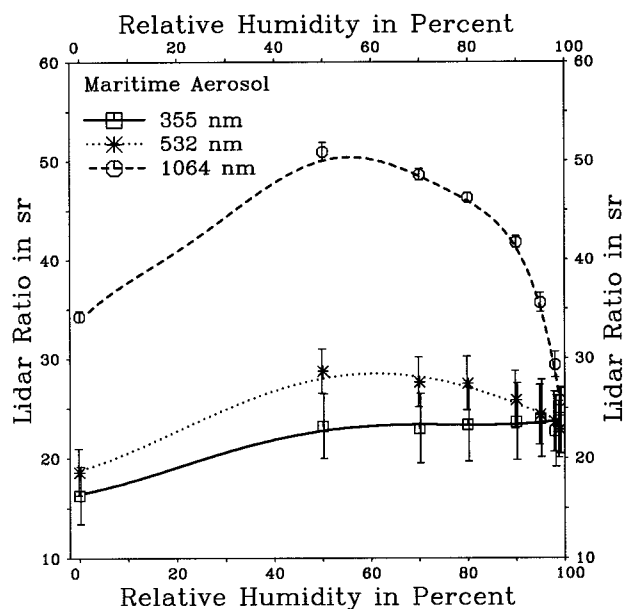


FIG. 4. Same as Fig. 3 but for maritime aerosol.

water soluble and the sea salt components grow with increasing relative humidity (see Table 2).

In this study, the water soluble component varies between 0.3 and 1 in steps of 0.1, the sea salt accumulation mode ranges between 2×10^{-3} and 2×10^{-2} (step width: 1.8×10^{-3}), and the sea salt coarse mode varies between 3×10^{-7} and 3×10^{-6} (step width: 2.7×10^{-7}). For every combination, the mixing ratio of the soot component is chosen to sum up all four mixing ratios to 1. This process yields maximum soot contents of nearly 0.7, a value that is somewhat higher than that of 0.576, which was proposed by Hess et al. (1998) for the aerosol type "maritime polluted." Since Hess et al. (1998) note the strong variability of the soot content over coastal areas, it seems appropriate to respect such high soot contents in a systematic analysis as well.

All calculations are repeated for eight different values of the relative humidity (see section 4), and the results for the mean lidar ratios \hat{S} and their standard deviations s are plotted in Fig. 4. The largest values of \hat{S} , which have remarkable small standard deviations, are calculated for 1064 nm. For the lidar ratio of maritime aerosol, the accumulation mode of the sea salt particles is the dominant component. This is caused by the median radii of the accumulation sea salt component, which, depending on the relative humidity, ranges between 209 and 995 nm, that is, the order of magnitude of the Nd: YAG wavelengths.

Since air masses of the PBL over oceans usually have relative humidities of more than 50%, it can be stated that the lidar ratio of maritime aerosol decreases with relative humidity for most atmospheric conditions. This decrease is a function of wavelength: for 355 nm, the

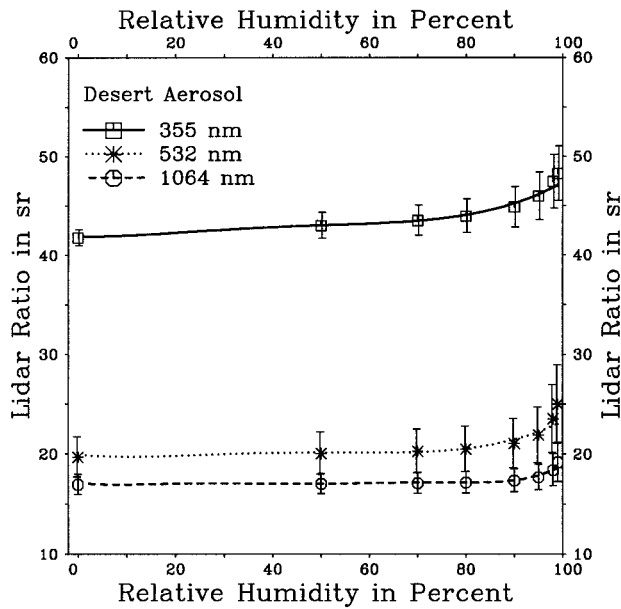


FIG. 5. Same as Fig. 3 but for desert aerosol.

variations of \hat{S} with f are nearly negligible, and for 1064 nm, the variability can be as high as 25 sr.

The calculated uncertainties of \hat{S} for maritime aerosol have less dependence on f than for the continental aerosol type: for 355 nm, the uncertainties range between $\pm 14\%$ and $\pm 18\%$; for 532 nm, they lie between $\pm 8\%$ and $\pm 13\%$; and for 1064 nm, the corresponding values are $\pm 1\%$ and $\pm 5\%$.

6. Desert aerosol

The desert aerosol originates from desert areas and mainly consists of the water soluble component and the nucleation, accumulation, and coarse particle mode of minerals. Since the mineral components do not change their physical-chemical properties with relative humidity, all changes of the lidar ratio of desert aerosol with the relative humidity result from the water soluble component.

The calculation of the lidar ratios is performed in the same manner as described in section 4. For the computations, the water soluble component varies between 0.6 and 0.9 (step width: 0.1), the mineral accumulation mode ranges from 1×10^{-2} to 4×10^{-2} (step width: 1×10^{-2}), and the mineral coarse mode lies between 5×10^{-5} and 8×10^{-5} (step width: 1×10^{-5}). The mixing ratio of the mineral nucleation mode is chosen to sum up the total mixing ratio to 1.

The calculated lidar ratios and their standard deviations are summarized in Fig. 5. The values of \hat{S} for 355 nm are about twice the values for 532 and 1064 nm. Similar to the dominance of the accumulation mode of sea salt for the lidar ratio of maritime aerosol, the lidar ratio of desert aerosol is governed by the mineral ac-

cumulation mode (median radius: 390 nm). Accordingly, the influence of the water soluble component is rather small: only for relative humidities of more than 90% is the lidar ratio considerably changed. Such atmospheric conditions are unlikely to occur over desert areas. Thus, the lidar ratios can be assumed to be independent of f for the majority of cases.

For all values of f , the sensitivity of \hat{S} due to changes of the desert aerosol composition is most pronounced for 532 nm. This is evident from the uncertainties of \hat{S} : for 355 nm, the uncertainty ranges between $\pm 2\%$ and $\pm 6\%$; for 532 nm, between $\pm 10\%$ and $\pm 16\%$; and for 1064 nm, between $\pm 6\%$ and $\pm 10\%$.

7. Empirical formula for $\hat{S}(f)$

The mean lidar ratios \hat{S} were discussed above for continental, maritime, and desert aerosol for eight different values of the relative humidity f . As mentioned in section 1, the information about the vertical profile of f can be deduced from radiosonde data. For practical applications, it is required that the corresponding mean values of the lidar ratio can be derived immediately from the vertical profile of f . On the basis of the results of sections 4 through 6, for each wavelength and each aerosol type, a power series expansion is performed for $\hat{S}(f)$:

$$\hat{S}(f) \approx \sum_{j=1}^J a_j f^{j-1}, \quad (7)$$

with a_j the polynomial coefficients and J the total number of the coefficients. The value of J is found by minimizing a least squares merit function (Press et al. 1992) and varies between 5 and 10 depending on the shape of the original function. The resulting coefficients are listed in Table 3.

To compare the polynomial fit with the input data, the fitted curves and the computed values of $\hat{S}(f)$ are plotted in Figs. 3–5 for continental, maritime, and desert aerosol, respectively. In all cases, the curves lie within the error bars of the computed lidar ratios, indicating that the power series expansions are mathematically sufficiently accurate.

A comparison between these results and the outcomes of the experimental studies mentioned in section 1 is rather difficult because of the different wavelengths used and in most cases the lack of information about the variability of the considered aerosols with relative humidity.

For continental aerosols, Salemink et al. (1984) report a stronger dependence of S on f , but their absolute values (25–70 sr) do not disagree with the values determined in this study. The data of Takamura et al. (1994) do not conflict with the results of this study, even if they determined low values of about 20 sr, too. The values of Waggoner et al. (1972) seem to be very high, even when a large soot content is assumed. Low values

TABLE 3. Coefficients for the power series expansions of the lidar ratio for different aerosol types.

	Continental			Maritime			Desert		
	355 nm	532 nm	1064 nm	355 nm	532 nm	1064 nm	355 nm	532 nm	1064 nm
a_1	4.252×10^1	4.531×10^1	4.093×10^1	1.646×10^1	1.884×10^1	3.387×10^1	4.191×10^1	1.993×10^1	1.706×10^1
a_2	4.400×10^{-1}	2.628×10^{-1}	7.091×10^{-2}	8.312×10^{-2}	1.277×10^{-1}	5.038×10^{-1}	-9.523×10^{-3}	-4.398×10^{-2}	-2.101×10^{-2}
a_3	-7.877×10^{-3}	-3.085×10^{-3}	2.006×10^{-3}	3.890×10^{-3}	5.191×10^{-3}	-1.675×10^{-2}	2.131×10^{-3}	2.865×10^{-3}	1.263×10^{-3}
a_4	1.395×10^{-5}	1.334×10^{-4}	1.767×10^{-5}	-8.203×10^{-5}	-1.037×10^{-4}	5.497×10^{-4}	-4.507×10^{-5}	-5.518×10^{-5}	-2.411×10^{-5}
a_5	7.881×10^{-6}	-2.356×10^{-6}	-6.958×10^{-6}	4.225×10^{-7}	4.364×10^{-7}	-3.393×10^{-6}	3.014×10^{-7}	3.430×10^{-7}	1.480×10^{-7}
a_6	-1.472×10^{-7}	1.412×10^{-8}	2.242×10^{-7}	0.	0.	-1.035×10^{-7}	0.	0.	0.
a_7	8.581×10^{-12}	0.	-2.708×10^{-9}	0.	0.	1.086×10^{-9}	0.	0.	0.
a_8	1.350×10^{-11}	0.	1.149×10^{-11}	0.	0.	2.185×10^{-12}	0.	0.	0.
a_9	-2.899×10^{-14}	0.	0.	0.	0.	-1.397×10^{-14}	0.	0.	0.
a_{10}	-3.411×10^{-16}	0.	0.	0.	0.	-2.345×10^{-16}	0.	0.	0.

ranging from about 21 to 32 sr are found by an earlier numerical study of McCormick et al. (1968), which neglected the wavelength dependence and the imaginary part of the refractive index (i.e., absorption) and assumed a Junge size distribution.

By a minimum search technique, Sasano and Browell (1989) determined the lidar ratio of maritime aerosol from multiple wavelength lidar observations. For 300 nm, they reported values ranging from 5.1 to 19.4 sr, which are somewhat lower than the values given in this study for 355 nm. However, from the wavelength dependence of S shown in Fig. 4, it seems that calculated values for 300 nm would lie close to the values reported by Sasano and Browell (1989). Their maximum value of 30 sr for 600 nm also agrees with the results of this study.

A comparison of the results for the desert aerosol with the outcomes of Spinhirne et al. (1980) provides a good agreement. Their retrieved value of 19.5 sr at 694 nm fits well with the values given in Fig. 5 for dry particles.

The measurements of Rosen et al. (1997) were taken at rural deserts, nearby mountains, and polluted areas under fair weather conditions after sunset. Thus, as a first-order approximation, their average values of 41.6 sr at 490 nm and of 32.2 sr at 700 nm can be regarded as a mean value of the lidar ratio for the continental and the desert aerosol. On the assumption of $f = 50\%$, Eq. (7) provides 51.9, 38.6, and 31.0 sr for 355, 532, and 1064 nm, respectively. Evidently, both the wavelength dependence and the absolute values are in close agreement with the data of Rosen et al. (1997). The same is true on the assumption of slightly higher or lower relative humidities than the arbitrary chosen value of 50%.

Thus, it is expected that the empirical formulation of $\hat{S}(f)$ via Eq. (7) with the coefficients listed in Table 3 will be a useful tool for an estimation of the lidar ratio for the Nd:YAG wavelengths. Nevertheless, it must be emphasized that other assumptions on the soot properties, on the shape of the mineral particles, on external versus internal mixtures of the aerosol components, and on the growth relations of the size distributions may affect the outcome of the lidar ratio calculations.

8. Concluding remarks

In this study, lidar ratios and their standard deviations for the continental, maritime, and desert aerosol with their dependence on relative humidity are presented. The variability of a distinct aerosol type is accounted for by variations of the mixing ratios of the corresponding aerosol components. All computations are performed for three Nd:YAG wavelengths: 355, 532, and 1064 nm. The model input is summarized in Tables 1 and 2, and the main results are plotted in Figs. 3–5.

Although a wide range of variability of tropospheric aerosols was covered in this study, there are remaining difficulties that can make the lidar ratio determination

doubtful even if the relative humidity along the measurement path is known.

First, as is clear from Fig. 2, there exist atmospheric conditions and hence mixing ratio combinations whose resulting lidar ratios differ considerably from an assumed mean value. This is especially true for a high soot amount and low relative humidities, as in the case of continental aerosol. This problem can only be eliminated by using larger wavelengths, where the influence of soot is slightly diminished.

Second, the simultaneous existence of different aerosol types in different heights above the measurement site prevents the evaluation of the lidar signal over the whole range domain. For example, over the oceans, the occurrence of the sea salt components is mainly limited to the PBL. Above the PBL, the aerosol composition is expected to be similar to that of continental aerosol but with a small amount of insoluble particles. In this case, the height of the PBL must be estimated from the lidar signal or the relative humidity profile. Accordingly, both parts of the measurement path, that is, the PBL and the free troposphere, are evaluated separately. Using the data of Hess et al. (1998) for a free troposphere with 50% relative humidity, the computed lidar ratios are 56.9, 58.4, and 51.3 sr for the wavelengths of 355, 532, and 1064 nm, respectively.

A similar problem can occur when mineral aerosol is transported from its source in the deserts to regions where other aerosol types are present. In that case the mineral particles form an aerosol layer above the aerosol layer of the PBL (Hess et al. 1998). By sedimentation, the aerosol components of both layers are externally mixed and thus the microphysical properties of the original aerosol layer are considerably changed. Under these conditions, a lidar ratio determination is ambiguous and useful results cannot be expected. For the mineral-transported component alone, from the data of Hess et al. (1998), the calculated lidar ratios are 22.0 (355 nm), 12.5 (532 nm), and 26.6 sr (1064 nm).

Another source of error is the inaccuracy of the relative humidity determined with the hygrometer of the radiosonde. These inaccuracies are mainly caused by the thermal lag and the solar heating of the instrument during the ascent. Both effects provoke an overestimation of f , and their strength depends on the actual state of the atmosphere. The mean relative humidity errors are 6% between 1013 and 700 hPa and 10% between 700 and 500 hPa (Pratt 1985). Thus, especially for large relative humidities, the accuracy of the lidar ratio determination is not only limited by insufficient a priori knowledge about the composition of the aerosols but also by the uncertainty of the relative humidity determination.

Acknowledgments. Peter Koepke and Peter Völger from the University of Munich are gratefully acknowledged for the delivery of aerosol data and the Mie code,

as well as for their fruitful comments. The comments of the two anonymous reviewers significantly improved an earlier version of the paper.

REFERENCES

- Bissonnette, L. R., 1986: Sensitivity analysis of lidar inversion algorithms. *Appl. Opt.*, **25**, 2122–2125.
- Bohren, C. F., and D. R. Huffman, 1983: *Absorption and Scattering of Light by Small Particles*. Wiley and Sons, 530 pp.
- d'Almeida, G., P. Koepke, and E. P. Shettle, 1991: *Atmospheric Aerosols: Global Climatology and Radiative Characteristics*. A. Deepak, 561 pp.
- Fitzgerald, J. W., 1984: Effect of relative humidity on the aerosol backscattering coefficient at 0.694- and 10.6- μm wavelengths. *Appl. Opt.*, **23**, 411–418.
- Hänel, G., 1976: The properties of atmospheric aerosol particles as functions of the relative humidity at thermodynamic equilibrium with the surrounding moist air. *Advances in Geophysics*, Vol. 19, Academic Press, 73–188.
- Hess, M., P. Koepke, and I. Schult, 1998: Optical Properties of Aerosols and Clouds: The software package OPAC. *Bull. Amer. Meteor. Soc.*, **79**, 831–844.
- Hughes, H. G., J. A. Ferguson, and D. H. Stephens, 1985: Sensitivity of a lidar inversion algorithm to parameters relating atmospheric backscatter and extinction. *Appl. Opt.*,
- Klett, J. D., 1981: Stable analytical inversion solution for processing lidar returns. *Appl. Opt.*, **20**, 211–220.
- , 1985: Lidar inversion with variable backscatter/extinction ratios. *Appl. Opt.*, **24**, 1638–1643.
- Kovalev, V. A., 1993: Lidar measurement of the vertical aerosol extinction profiles with range-dependent backscatter-to-extinction ratios. *Appl. Opt.*, **32**, 6053–6065.
- McCormick, M. P., J. D. Lawrence, and F. R. Crownfield, 1968: Mie total and differential backscattering cross sections at laser wavelengths for Junge aerosol models. *Appl. Opt.*, **7**, 2424–2425.
- Pratt, R. W., 1985: Review of radiosonde humidity and temperature errors. *J. Atmos. Oceanic Technol.*, **2**, 404–407.
- Press, W. H., S. A. Teukolsky, W. T. Vetterling, and B. P. Flannery, 1992: *Numerical Recipes in FORTRAN*. Cambridge University Press, 963 pp.
- Rosen, J. M., R. G. Pinnick, and D. M. Garvey, 1997: Measurement of the extinction-to-backscatter for near-surface aerosols. *J. Geophys. Res.*, **102**, 6017–6024.
- Salemink, H., P. Schotanus, and J. B. Bergwerff, 1984: Quantitative lidar at 532 nm for vertical extinction profiles in the lidar solution. *Appl. Phys.*, **34B**, 187–189.
- Sasano, Y., and E. V. Browell, 1989: Light scattering characteristics of various aerosol types derived from multiple wavelength lidar observations. *Appl. Opt.*, **28**, 1670–1679.
- , —, and S. Ismail, 1985: Error caused by using a constant extinction/backscattering ratio in the lidar solution. *Appl. Opt.*, **24**, 3929–3932.
- Shettle, E. P., and R. W. Fenn, 1979: Models for the aerosols of the lower atmosphere and the effects of humidity variations on their optical properties. Air Force Geophysics Laboratory Environmental Research Papers 676, AFGL-TR79-TR79-0214, 94 pp. [Available from Air Force Geophysics Laboratory, Hanscom AFB, Massachusetts 01731.]
- Spinhirne, J. D., J. A. Reagan, and B. M. Herman, 1980: Vertical distribution of aerosol extinction cross section and inference of aerosol imaginary index in the troposphere by lidar technique. *J. Appl. Meteor.*, **19**, 426–438.
- Takamura, T., Y. Sasano, and T. Hayasaka, 1994: Tropospheric aerosol optical properties derived from lidar, sun photometer, and optical particle counter measurements. *Appl. Opt.*, **33**, 7132–7140.
- Waggoner, A. P., N. C. Ahlquist, and R. J. Charlson, 1972: Measurement of the aerosol total scatter-backscatter ratio. *Appl. Opt.*, **11**, 2886–2889.